Instrument Science Report ACS 2022-06

ACS/WFC CTE photometric correction: improved model for bright point sources

Marco Chiaberge and Jenna Ryon
December 19, 2022

ABSTRACT

We present an updated model to correct aperture photometry of point sources for CTE losses. The model is similar to the CTE photometric correction currently available but with a few major improvements that allow more accurate results for bright stars. The standard CTE photometric correction uses a linear dependence on source brightness, background level and time. Here, we present the improved model using a curvilinear dependence on point source brightness. The overall statistical accuracy of the new model is as good as, or better than the previous one. In this ISR we present the data analysis and describe the data science modeling.

1. Introduction

CCDs in space are exposed to radiation damage, which can strongly decrease the Charge Transfer Efficiency (CTE). Imperfections in the crystalline lattice of the CCD increase due to the bombardment of energetic charged particles in the space environment (Pickel et al. 2003, Srour et al. 2003, for reviews). This generates an increasing number of charge traps that lower the CTE of each pixel of the detector. CTE is defined as (1-CTI), where CTI = $\Delta Q/Q$ is the fractional charge lost during each single transfer (Charge Transfer Inefficiency). A perfect CCD would have CTE=1 (CTI=0).

CTE has been regularly monitored in ACS/WFC since launch in a number of different ways, including both external and internal observations (see Chiaberge ISR-ACS 2012-05, Ryon et al. ISR-ACS 2018-09, Anderson & Ryon ISR-ACS 2018-04). Here we report on the latest update to the photometric CTE correction for point sources, which is based on external observations of the 47 Tucanae globular cluster. Calibration observations are part of the ACS calibration plan routine programs. Data are collected once every HST Cycle. The original correction model (Reiss & Mack ISR-ACS 2004-06) was substantially changed and improved in 2012 (Chiaberge ISR-ACS 2012-05, hereinafter C12). Model coefficients are updated every Cycle to allow for accurate time-

dependent correction of point-like fluxes. Because of both the increased CTI, and the larger amount of data available, we recently noticed behaviors that were previously not visible. This ISR reports on the recent modifications we have applied to the model to take into account these new findings.

2. Observations and data reduction

The target of the observing program is a field ~7' West of the core of the globular cluster 47 Tucanae. We image the target field with WFC at the initial position (image "0"), and then we re-image the field twice, after conducting large slews (102"), i.e., half the size of the WFC detector. The slews are performed once in the X and once in the Y directions in the detector framework, to vary the number of transfers for each star in the field and to check both serial and parallel CTE, respectively. Here we only utilize the slews along the Y direction (image "1"), since the X-CTE is still an order of magnitude smaller than the Y-CTE, and hard to accurately measure. Images are taken using two different filters (F502N and F606W) and with a range of exposure times (30, 150 and 400s), in order to sample different background levels. A region closer to the center of the cluster is also imaged to derive a dataset at low background but with a large number of stars to improve the statistics. Usually, data for at least six background levels are obtained. For a more extensive description of both the characteristics of the datasets and the method for the data analysis, we refer the user to C12. In the following we summarize the main steps.

The data considered in this ISR for the purpose of deriving the updated correction model were collected as part of the ACS calibration plans for Cycles 17 through 28. Data up to Cycle 19 were presented in C12. The Calibration program IDs for Cycle 20 through 28 are 13155, 13592, 13955, 14398, 14507, 14949, 15522, 15760, 16380.

In recent cycles we have faced a number of observational failures mostly related to guide star issues. In general, failed observations for the external CTE monitor program cannot be repeated since it is mandatory to use the exact same guide stars, and those are usually available only for a very short period of time. The only possibility would be to repeat the entire program. This is generally not considered as an option, unless the entire program fails and/or new data are missing for more than two consecutive Cycles. In Cycle 24 (ID 14507) one dataset (i.e., one background level) was not sampled because the shutter remained closed. In Cycle 25 (ID 14949) only two datasets (i.e., two background levels) were usable. In that case, updated model parameters were not derived and it was only checked that the previous model was still accurate. In Cycle 28, due to a series of failures and problems with guide stars on the standard target, we were forced to switch to a similar field around Omega Centauri. Unfortunately, even in that case, problems with guide star acquisitions affected the observations as we obtained only 3 out of the 6 datasets originally planned. The Omega Cen data have a higher background level, likely because of the higher zodiacal light but possibly also because the target is a significantly richer globular cluster. However, the images can still be included in the analysis and also provide an important consistency check at higher background levels as compared to those achieved in 47 Tuc.

Observations up to Cycle 25 were processed as described in C12. In brief, images were registered using Tweakreg and Astrodrizzle, and photometry was performed on DRZ files. Data from Cycle

26 to 28 were processed using the CTE pipeline described in Miles & Chiaberge ACS-TIR 2019-01. The major difference in the latter method is that photometry is now performed on CRJ files (i.e., calibrated, CR-SPLIT combined, but not corrected for geometric distortion) and then the pixel area map is applied to properly weight each pixel by its area on the sky. This new strategy has shown to return significantly more precise (less noisy) results. In the near future, the ACS team is planning on re-reducing all data taken as part of the External CTE monitor programs with the Miles & Chiaberge pipeline, and re-evaluating the model to determine whether any further accuracy improvements are achievable due to the enhanced precision of the photometry.

3. Data analysis and results

For each epoch, filter and exposure time combination, stars are grouped in bins of stellar brightness (in e^-) measured in each "pair" of images (0,0 and 0,1). Each star is assigned to a particular bin based on the highest brightness measured in each "pair". Six or more bins are obtained for each of the datasets (i.e. for each background level, at each epoch). A non-weighted linear fit to the data is performed and the value of Δmag_{2000} (difference in magnitude for 2000 pixel Y-transfers) is derived from the slope of the linear regression, after iterative rejection of outliers. Note that we chose 2000 pixels to track the losses at the edge of the chip both for simplicity and because the magnitude of a star centered at the extreme edge of the chip (corresponding to 2048 transfers) cannot not be accurately measured. In Fig. 1 we show the results for 6 bins of stellar flux derived from the images taken with F606W and 40 sec exposure time in Cycle 26 (July 2019). The selected range of sky background for the data in the figure is between 5 and 7 electrons.

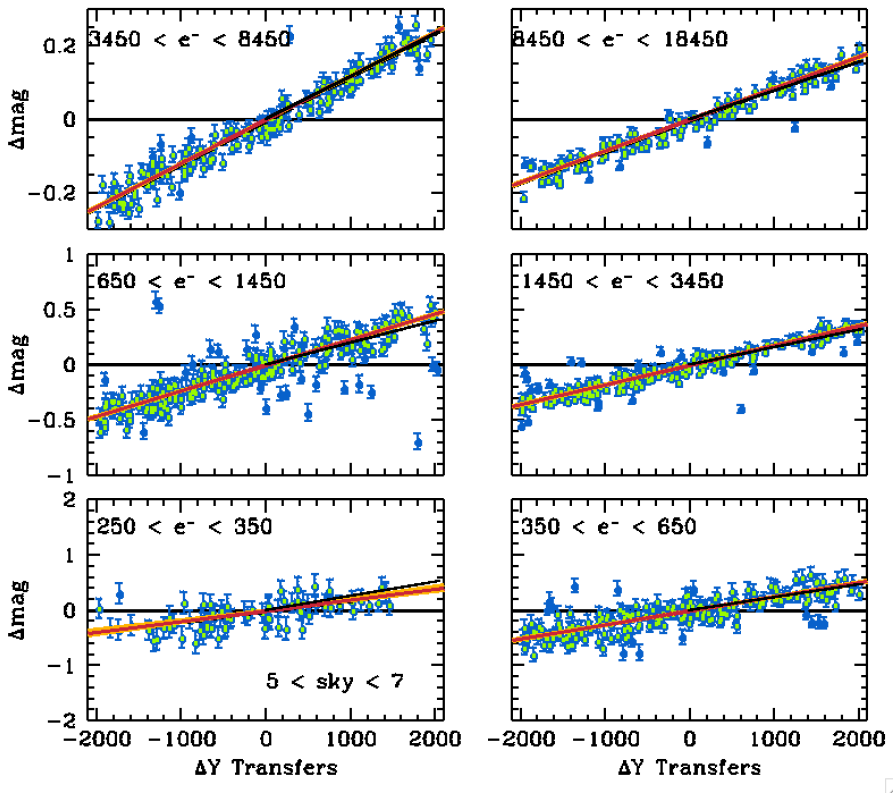

Figure 1 Magnitude losses for different bins of stellar brightness (in e^- within a 3-pixel aperture) and different levels of sky background. Δmag is the difference between the magnitudes measured in images taken at position "0" and "1". ΔY-transfers is the difference in number of pixel transfers for each star between image "0" and image "1" (see text). Data are from Cycle 26, July 2019, F606W, with an exposure time of 40s. Filled blue circles are rejected outliers. The black dashed lines (where visible) are linear fits to the data, and the red line is the same fit shifted so that the value of the intercept is 0. The yellow lines correspond to 1-σ error on the slope of the fit. Yellow lines are visible only in the lower panels because of the very small rms at higher fluxes. The considered bin of stellar brightness is reported in the top left corner of each box.

3.1 CTE dependence on stellar brightness: new findings

The linear dependence between Δmag_{2000} and Log Brightness [e^-] has been well known since the work of C12. Significant deviations from a linear relation have been observed at the lower end of the stellar flux distribution because of incompleteness (see Fig. 3 in C12). At the higher end, no deviation from a linear relationship was observed until about Cycle 25. In this regime, both saturation for the long exposures and lack of a sufficient number of bright stars for the short exposures prevents enough exploration of the paramenter space to achieve a comprehensive picture. In Fig. 2 we show the magnitude loss for stars located at Y=2000 transfers against stellar brightness measured in e^- within a 3-pixel aperture radius. The trend showing a substantial increase of CTE losses with time is clearly visible. Note that in C12 we referred to the latter quantity as *flux*

in units of electrons, both for historical reasons and because the photometry was always performed on DRZ images, which have units of $e^- s^{-1}$. However, while we refer to the exact same quantity here, it is more appropriate to define it as *brightness* (or *fluence*) in electrons.

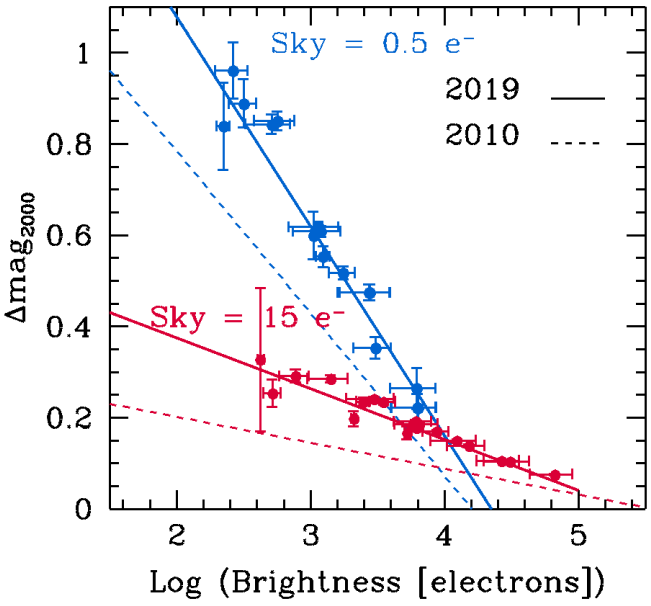

Figure 2 Magnitude loss at the edge of the chip at Y=2000 transfers, as a function of the Log of stellar brightness, measured in electrons within a 3-pixel aperture radius. The solid lines are from observations taken in 2019 (Cycle 26, Program ID CAL/ACS 15522), the dashed lines are the best fits from the 2010 dataset (Cycle 18, CAL/ACS 12385). Blue is for the lowest background, red for an average background of ~15 electrons. The error bar in the x-axis represents the width of each stellar brightness bin. The bin's width generally depends on the number of stars available in each bin, although in some cases different bin sizes are explored. On the y-axis the error bar is the rms of the residuals for each datapoint.

In recent Cycles the worsening of the CTE coupled with the improved pipeline has allowed us to determine that a flattening of the CTE loss at the highest fluxes is present. This is reasonable to expect, since a simple linear extrapolation towards fluxes higher than those sampled by these data would imply CTE losses near to zero or even negative losses, which would be unphysical. Furthermore, bright stars have a lot of electrons outside the 3-pixel aperture radius. These act as an increased background level, which locally increases CTE for those stars.

In Fig. 3 we show the CTE mag losses at the edge of the chip vs the brightness of the stars as measured by the log of the electrons within a 3-pixel aperture radius. Differently from what is shown in Fig. 2, at Log e^- > 4 the linear dependence deviates from simple linearity, and the losses seem to follow a broken power law. In other words, bright stars undergo higher CTE losses than the prediction from a simple linear model. This is mostly apparent for lower background levels, while at the highest background a linear model is still able to accurately reproduce the data. While such a pattern makes physical sense, it was not obvious until Cycle 27. In the figure, we show two different background levels (0.7 and 6 e^- in blue and green, respectively). Linear models corresponding to each of these are shown with dashed lines. These are the linear models from C12 obtained using the most updated coefficients, which include observations from Cycle 27. The dashed yellow line is the model for a background of 50 e^- and it is shown with no datapoints (only for reference). All the model lines intersect at around Log e^- ~ 4.4. While datapoints are not available for the blue background because bright stars are missed in those observations, the green data clearly flatten onto the yellow line after this inflection point. A similar behavior is seen for

the other background levels.

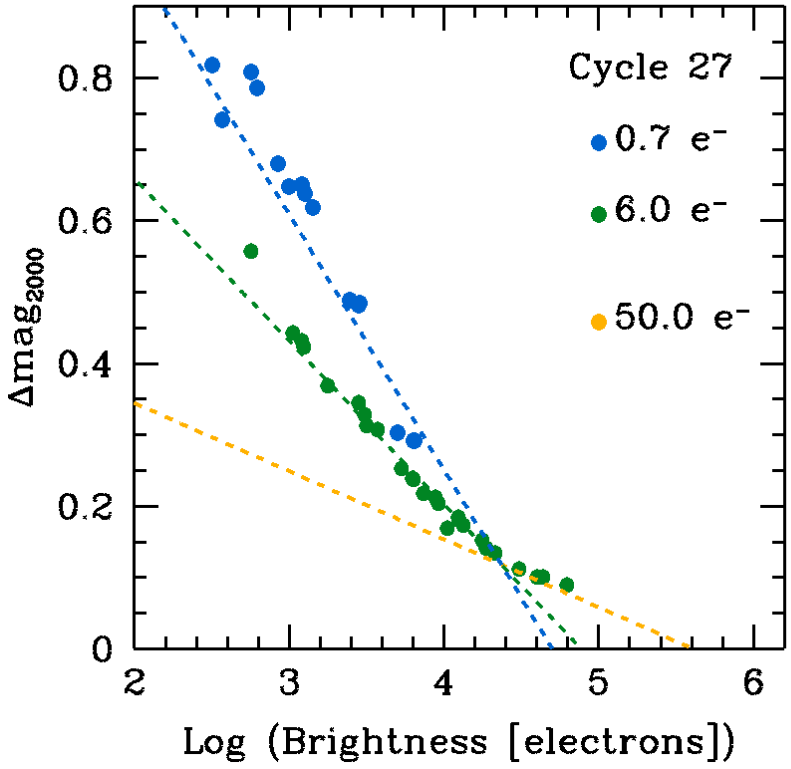

Figure 3 CTE losses at Y=2000 pixel transfers against Log of stellar brightness measured within a 3-pixel aperture radius. Green and blue data refer to two different background levels from the Cycle 27 dataset. The dashed lines are linear models from C12 using the most up-to-date coefficients. The yellow model is plotted with no data only for reference.

3.2 CTE dependence on sky background: the impact of the dark current

CTE losses also strongly depend on the background level. The important parameter is not the average sky level in the image but the actual local background measured near each stellar source. However, recently we found evidence that the dark current should be added to the sky level in order to better model for the CTE losses. Dark current is removed during pipeline processing of the data, but it is present when the readout takes place. Therefore the amount of charge accumulated as dark current during the exposure can be important for CTE losses. Again as for the effect described in the previous section, this has become clear only as CTE degraded to a sufficient level and as ambient dark current has slowly risen.

For the purpose of explaining this finding, let us ignore for the moment the latest results discussed in Sect 3.1. We then assume as in C12 that magnitude losses at Y=2000 can be described using the

following linear relation:

$$\Delta mag_{\Delta y=2000} = \alpha \, Log(electrons) + \beta,$$

where both α and β are coefficients that linearly depend on the background level (see C12 for more details).

We now know that this is an approximation that is only valid for stars below a certain brightness (see previous Section). However, for the purpose of investigating the effect of the background level on CTE we use this simplified representation.

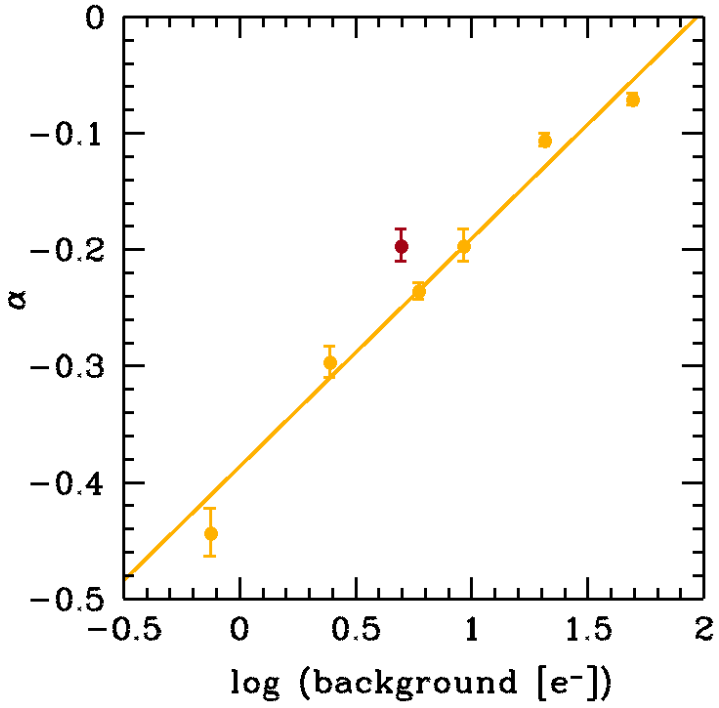

Figure 4 Linear dependence of the α parameter on the background level. The yellow points include the dark current. The red point is from F502N 360s dataset without dark current, which is the only dataset for which the inclusion of the dark current is significant. The line is a weighted linear fit to the yellow data points. Data from Cycle 27.

In Fig. 4 we show the linear relationship between α and the background. The yellow points correspond to each of the six background bins derived from the observations in Cycle 27. The yellow points in this plot include the dark current. The red point is the datapoint derived from the observations taken with F502N and 360 s exposure time, when the dark current is not included. It is clear that the inclusion of the red point instead of the one immediately to its right, which corresponds to the exact same dataset, would introduce a significant error in the model best fit. This is the only dataset in the External CTE monitor calibration programs that is heavily affected by the dark current. In this case, the dark current accumulated during the 360s exposure more than

doubles the background level, which goes from ~ 4 electrons to 9. In all other cases, the effect of dark current is negligible. For example, in the other long exposure (400s) taken with F606W, the dark current only represents ~10% of the total background.

We now include the dark current in the data used to derive the model, for the sake of accuracy.

Users should consider whether the dark current is significant in their data, as compared to the sky level. If that is the case, they should add the dark current to the sky level for use in the model equation when estimating CTE losses. Note that the pixel-based CTE correction within CALACS is performed prior to dark subtraction, and thus accurately accounts for the additional filling of charge traps by exposure-integrated dark current.

4. Data science modeling

In order to include the new findings described above in the CTE photometric correction model, and in particular the flattening of CTE losses at high stellar brightness, we utilize the softwae package *R* (*R* Core Team, 2021) and data science modeling techniques.

The dataset is composed of a data frame of vectors with background level, stellar brightness, observation date, and magnitude loss at Y=2000, derived as described in C12. The use of Δmag_{2000} for each bin of stellar brightness and background level is justified by the significantly higher accuracy of this method, as compared to conducting a global fit with the results from single stars and also including the number of Y-transfers in the model. We know that CTE losses are adequately modeled with a linear relation across the WFC chip, and this significantly reduces the noise, leading to a much more statistically accurate model. While we did attempt a global fit in the past few years, we decided not to use that approach given the poor results obtained.

We also do not consider the error on Δmag_{2000} as we do not apply *weights* to the linear model. Great care is given to outlier rejection before (and after) the final dataset is ingested in the model. Datapoints with error greater than ~10% of the mag loss are rejected immediately, as they are mostly derived from bins with a small number of stars, therefore the statistical significance is very low.

During the work to derive the model, we utilize R to identify potential problems with outliers that were not rejected in advance, by plotting e.g. residuals vs fitted values (see Fig. 6 in C12). When an outlier is identified, we inspect the original data to check whether the datapoint is reliable. When problems are identified we remove this additional point from the dataset. This is not done very often, and only after the model is sufficiently convincing, in order avoid skewing the results by artificially eliminating data that do not fit our expectations. However, for example this technique was succesfully used to identify a number of points at low brightnesses that are still affected by

the well-known incompleteness effect in faint stars and were not spotted by eye.

The starting model is the result of C12, i.e.

$$\Delta mag_{2000}\ (MJD, SKY, F) = \qquad (1)$$

$$[p_1\ Log(SKY)\ Log(F)\ MJD\ +\ p_2\ Log(SKY)\ Log(F)\ +\ p'_1\ Log(SKY)\ MJD\ +q_1 Log(F)\ MJD\ +\ p'_2\ Log(SKY)\ +\ q_2 Log(F)\ +\ q'_1\ MJD + q'_2],$$

where MJD is the Modified Julian date of the observations, SKY is the background level in e^- per pixel (including dark current), and F is the star brightness in electrons within a 3- or 5-pixel aperture radius, depending on the users' preference. Note that for isolated, relatively bright stars a 5-pixel aperture may be better to improve the S/N.

As advertised in the ACS Instrument CTE website[1], initially p_1 and p'_2 had non-zero value, However, they were later set to zero since the statistical evidence for those two parameters being different from zero is negligible. We refer to this as model (1), in the following.

While the linear model (1) still produces a satisfactory fit (residual standard error ~ 0.03 mag) for data that lie within the majority of the parameter space, it fails for bright stars. The mismatch is particularly large at lower backgrounds, as explained in Sect. 3.1. This is shown in Fig. 5, with data from Cycle 27.

[1] https://www.stsci.edu/hst/instrumentation/acs/performance/cte-information

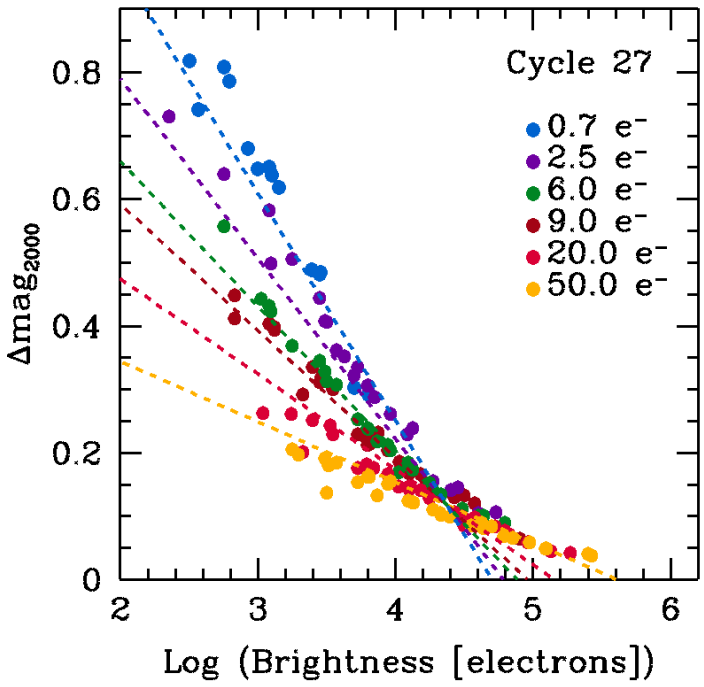

Figure 5 Magnitude losses at the edge of the chip, far from the amplifiers (Y=2000 pixel transfers) measured in Cycle 27 for six different sky background levels. The brightness is measured in electrons with a 3-pixel aperture radius. Different colors correspond to different backgrounds, as shown in the figure. The dashed lines are linear models for each background level, as derived from model (1). Errors are not plotted for clarity.

One of the major complications with deriving a model that is accurate for bright stars as well as for stars of intermediate and low brightness, is that the number of bright stars (those with more than 10^4 e^-) is small. Part of that is due to the fact that very bright stars are CCD-saturated in the image, and therefore are rejected. However, saturation happens at a brightness corresponding to ~ $10^{5.5}$ e^- (as usual this is measured within a 3-pixel aperture radius). Furthermore, the number of bright stars in the target cluster is smaller than the number of fainter stars. Therefore, the model is biased against the brightest stars. Changing the model only to include a flattening at high brightness does not solve the discrepancy, because CTE losses also depend on background level.

For the sake of both clarity and concision, we do not describe in detail all the attempts that were made using different CTE correction models in this ISR. However, we describe the steps undertanken and the reasoning behind the final determination of the model.

Since the effect we wish to reproduce is a flattening at high stellar brightness, a curvilinear model is needed. Therefore, we need to include a component proportional to 1/(Log brightness)^n. In the *R* notation, this means that the model will include one or multiple terms of the kind `I(1/lf^n)`. The I function in *R* isolates the content within parenthesis and treats it as is and not as an operator

within the formula. After running *R* numerous times, it was determined that a combination of terms with n=1 and n=2 return the best results in reproducing the observed shape.

However, the dataset from the observations does not include datapoints at very high brightness, particularly for the lower background levels. Saturation in the longest exposures and lack of sufficiently bright stars in the shorter exposures prevent these data points from being obtained. Therefore, the model is basically unconstrained at the brightest edge of the parameter space, and does not reproduce the few available datapoints well. In order to *hard constrain* the model behavior in such region of the parameter space, we include a small number of synthetic datapoints. This has the effect of forcing the regression computation to model the observed values correctly. This is done not only at high but also at very low brightness levels, since the new term in the model would otherwise bring the CTE losses to zero for faint sources, which is unphysical. We were extremely conservative when including these artificial dataset not to change the results for the parameter space covered by the observations. In the end, the *synthetic* data are only ~30 datapoints where the full dataset includes more than 1300. We wish to stress that these additional datapoints are only meant to constrain the model to behave in a way that is physically meaningful both in the range spanned by the obervations and at the extremes of the parameter space. They could simply be interpreted as boundary conditions.

In Fig. 6 we show the data from Cycle 20 and Cycle 27, with the added *synthetic* datapoints (black squares). Note that at high brightness the *synthetic* data have the same CTE loss value, independently of the background level, to be consistent with the observed pattern. In Cycle 20 *synthetic* data at both low and high stellar brightness were added. For Cycle 27 *synthetic* data at low brightness were not needed since the model already behaved sufficiently well in that regime (i.e. CTE losses increase as brightness decreases), even if the exact behavior is unknown. The data at low brightness are chosen to be on the extrapolation of the linear model (1).

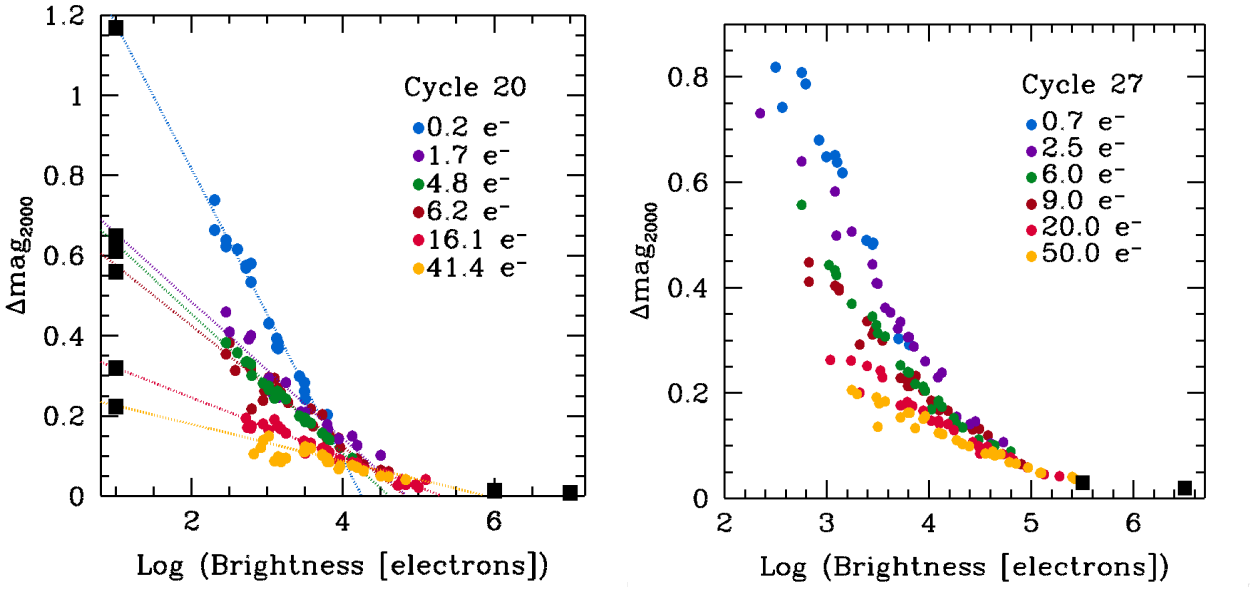

Figure 6 CTE losses at the edge of the chip (Y=2000 transfers) from Cycle 20 (left) and Cycle 27 (right). Different background levels correspond to different colors, as shown by the labels in each panel. The additional *synthetic* datapoints are shown as black squares. In the Cycle 20 datasets, additional datapoints are added both at low and high brightness. The *synthetic* data at low brightness lie on the extrapolations of the linear model for each background level (shown as dotted lines in the left panel only). At high brightness, the value of the CTE loss is assumed to be the same at all background levels, in agreement with the behavior shown by few observed datapoints in that regime.

With the inclusion of the *synthetic* data, we iteratively run *R* and derive the best model to fit the entire dataset. A large number of iterations were needed to find a satisfactory model. Data cleaning was also performed, by inspecting *R* plots (e.g. standardized residuals and leverage, as shown in C12) and iteratively checking the original data for reliability. Data that were deemed unreliable were eliminated. At the end of the process, our best fit is obtained with the following model

$$\Delta mag_{2000}(MJD, F, SKY) = a_1\,Log(SKY) * MJD * 1/Log\,F + a_2\,MJD * 1/(Log\,F)^2 + a_3\,1/(Log\,F) + a_4 Log(SKY) * 1/(Log\,F)^2 + a_5\,Log(SKY) * Log\,F + a_6\,1/(Log\,F)^2 + a_7\,Log\,F + a_8 Log(SKY) + a_9 \quad (2)$$

where the variables are defined as for model (1). The model is normalized at Y=2000 pixel transfers; therefore, the value of Δmag_y can be obtained using $\Delta mag_Y = \Delta mag_{2000} * (Y/2000)$, where y is the distance (in pixels) of the center of the measured point source to the amplifiers. For a star located on the WFC2 chip, Y is simply the y coordinate of the point source in the FLT frame. For WFC1, Y = (2049-y), where y is the y-coordinate (see C12, CTE correction cookbook section).

In Tab. 1 we report the coefficients a_i as derived for all datasets up to Cycle 28, with errors from *R*. Note that since the data are clustered we used the *lm.robust* function, which is part of the

estimatr package in *R*. For the error analysis, we assumed clustering in time (observation MJD), which results in the largest error estimates. This might not be the only source of clustering in our dataset, but we found that time is the parameter that has the largest impact on the error estimate.

The value of each coefficient will be updated every cycle and posted on the ACS CTE webpage (see footnote 1, Sect. 4). The Photometric CTE calculator (also at the above link) is periodically updated to the latest model and the latest coefficients.

In Fig. 7 we show the data with the new curvilinear models from two epochs, Cycle 20 and Cycle 27, corresponding to October 2012 and September 2020, respectively. As for Fig. 6, we plot CTE losses at the edge of the chip as a function of stellar brightness and for different background levels. The models are plotted as dashed lines, and each color corresponds to each background level. The small offset at the bright end of the parameter space (lower right tail) is in line with the overall accuracy of the model and is not a concern, as discussed in Section 4.2.

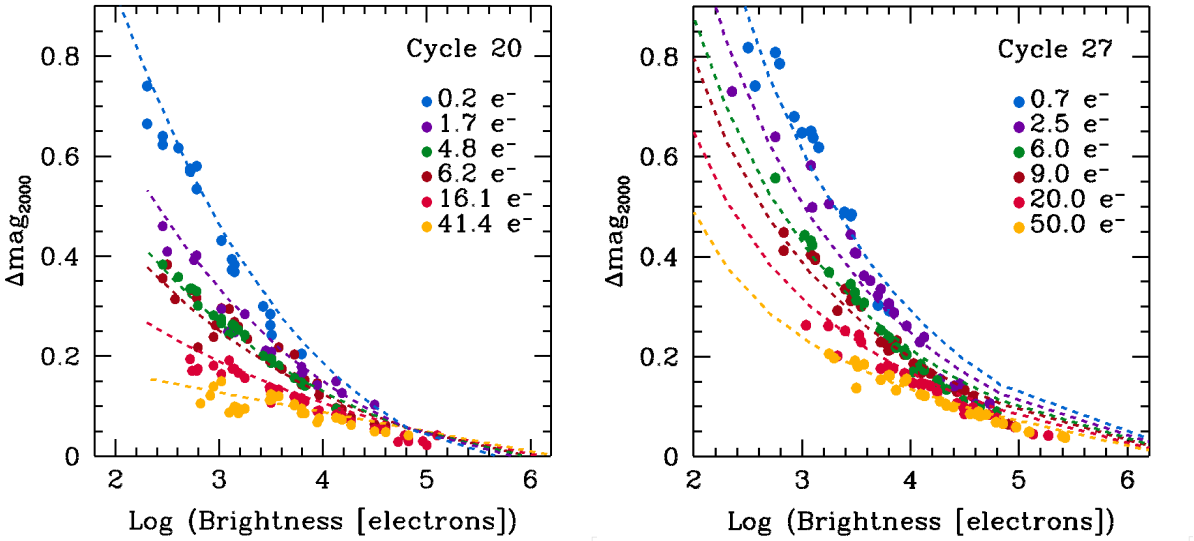

Figure 7 CTE losses at the edge of the chip (Y=2000 transfers) from Cycle 20 (left) and Cycle 27 (right). Different background levels correspond to different colors, as shown by the labels in each panel. Models are plotted as dashed lines, and each color corresponds to each background level.

4.1 Cycle 28 data

The dataset and model fitting presented here also include data from Cycle 28. As explained in Section 2 the Cycle 28 observations targeted Omega Centauri instead of 47 Tucanae, because of scheduling and guide stars problems. Furthermore, only a subset of the data is available, since some of the observations failed and could not be repeated. Moreover, the background levels are significantly higher than those returned by our standard target 47 Tuc with the exact same filter/exp time combinations. We show in Figure 8 the models applied to that specific dataset for reference. This dataset also serves as a verification of the accuracy of the model, since the observations used

a different target (Omega Cen vs. the standard 47 Tuc field), and a different range of background level.

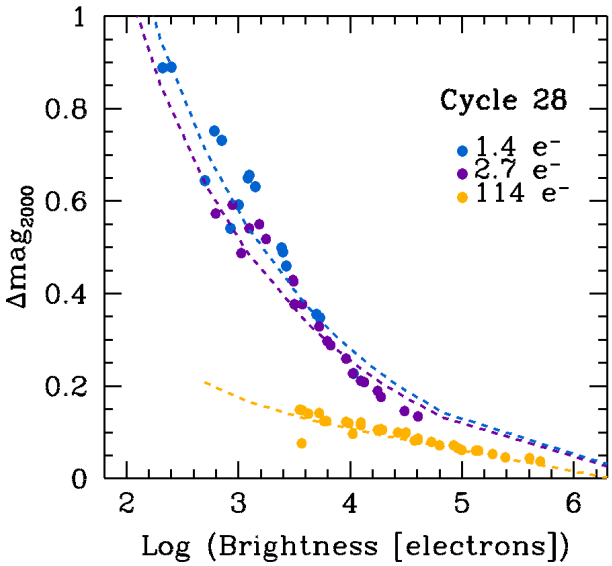

Figure 8 CTE losses as a function of stellar brightness and background level from Cycle 28 observations of Omega Centauri. As in Figs 5, 6, and 7, the background level is indicated with different colors.

Coefficient	Estimated value	Std. Error
a9	-1.265159e+00	1.532776e-01
a8	9.256621e-01	6.545480e-02
a7	7.319529e-02	2.225933e-02
a6	-4.178581e+01	1.523188e+00
a5	-6.832897e-02	9.490743e-03
a4	2.126813e+00	1.241196e-01
a3	5.374863e+00	3.557038e-01
a2	6.823563e-04	2.424278e-05
a1	-5.897623e-05	2.792799e-06

Table 1 Parameters of the curvilinear model for 3-pixel aperture radius photometry updated after the Cycle 28 Observations, obtained using the *R* function *lm_robust*. Adjusted R-squared = 0.9621 (a measure of the goodness of the fit, where a value of 1 means that the model perfectly predicts values), and model p-value = 3.677e-15. The full output table from *R* is provided in the Appendix.

4.2 Error estimate

The model outlined in the previous sections allows for an estimate of the CTE loss based on time of the observation, brightness of the star/point source on the image, background level (including dark current, if significant), and distance to the amplifier. However, we should keep in mind that the model is not perfect and while its accuracy keeps getting checked and updated every cycle, there is an error associated with the CTE loss estimate. Especially when measuring a source that is outside of the region of the parameter space covered by the observations, it is strongly

recommended to take a conservative approach and not assume that the estimate provided by the model corresponds to an exact value.

The residual standard error of the model's prediction can be calculated depending on the input parameters. In Fig. 9 we show the residual standard error of the model, for the region of the parameter space spanned by the calibration observations. Quoted errors correspond to the 95% confidence level and are calculated for the worst case scenario of a point source located at Y=2000, far from the amplifier. MJD=59414 (July 19th 2021) is used as a reference date. We do not recommend the users to add these errors to the measurement error in quadrature, but to use them as reference values to estimate the reliability of the correction for the specific parameters of the observation. As an example, for bright stars superimposed over a high sky level, the 0.01 mag residual error refers to the fact that the model slightly overpredicts the CTE losses (by about 1% at the edge of the chip, far from the amplifiers).

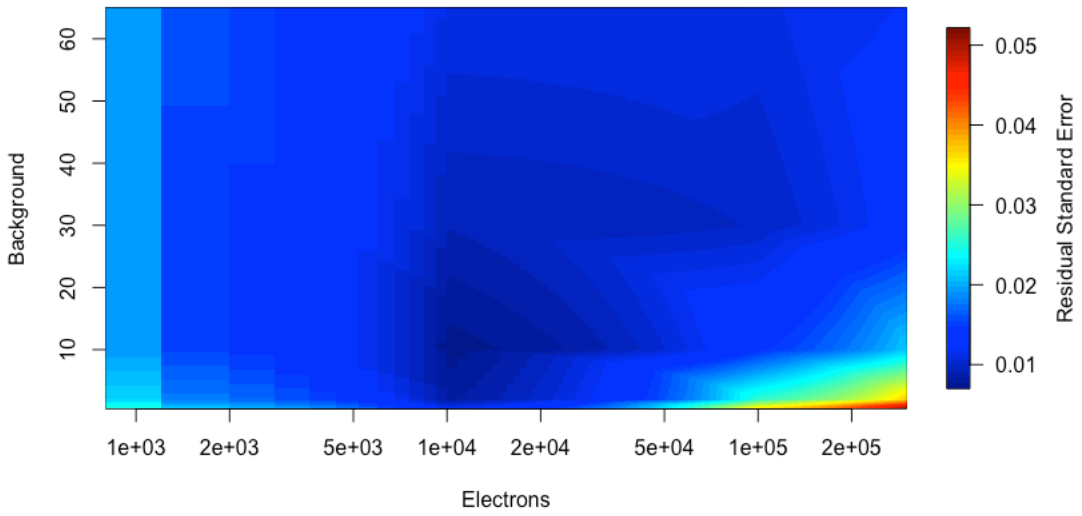

Figure 9 Residual standard error (in magnitudes) of the model for r=3 pixel aperture radius, for MJD=59414. The x axis reports the stellar brightness in electrons (number of e^- within r=3 pixel aperture). Y axis is background, in e^- per pixel.

4.3 Model parameters for photometry with a 5-pixel aperture radius

We used the same model and the same approach to derive a correction for users who prefer a slightly larger aperture radius. This might be more appropriate in some cases, for example for bright point sources. Also in this case we used a small set of synthetic data to force the model to avoid unphysical solutions in the region of the parameter space where datapoints are scarce, or absent. In Figs. 10 and 11 we show CTE losses at the edge of the chip, far from the amplifiers, as a function of stellar brightness. In Tab. 2 we report the coefficients for this model and the

parameters of the statistical significance for each coefficient and the full model.

Note that CTE losses for a 5-pixel aperture radius are smaller than for 3 pixels, since some of the charges that are lost in the CTE *trail* are recovered using a 5-pixel radius.

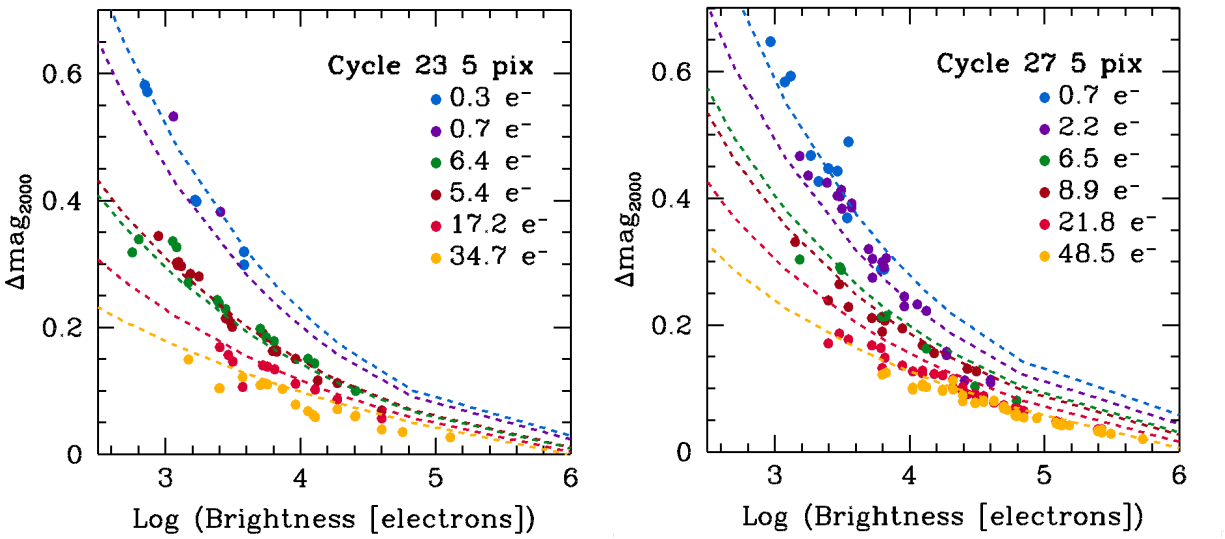

Figure 10 Magnitude losses as a function of stellar brightness, measured in electrons within a 5-pixel aperture radius. Data are from Cycle 23 (August 2016) and Cycle 27 (September 2020). The dashed lines are models. Each color corresponds to a different background level.

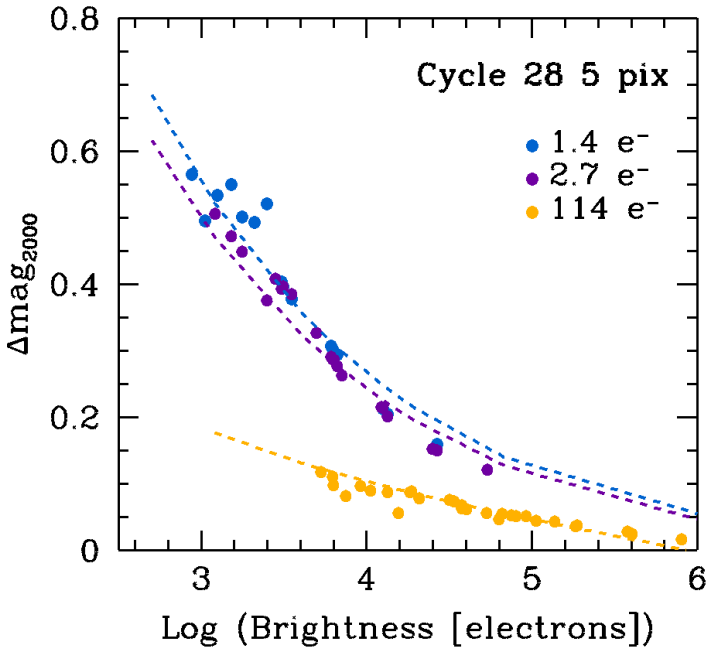

Figure 11 CTE losses vs log of stellar brightness for the Cycle 28 observations of Omega Centauri. Models

(dashed lines) and observations are reposted for aperture photometry using a 5-pixel aperture radius. Different colors correspond to different background levels. Compare with Fig. 8 for the same datasets but for photometry with a 3-pixel aperture radius.

Coefficient	Estimated value	Std. Error
a9	-1.683948e+00	3.779090e-01
a8	9.454385e-01	2.139650e-01
a7	1.191812e-01	3.962576e-02
a6	-4.957360e+01	5.696962e+00
a5	-7.861311e-02	2.076082e-02
a4	1.907908e+00	4.761967e-01
a3	6.615735e+00	1.077040e+00
a2	7.894505e-04	9.064712e-05
a1	-5.627863e-05	1.090462e-05

Table 2 Parameters of the curvilinear model for 5-pixel aperture radius photometry updated after the Cycle 28 observations, from the *R* function *lm_robust*. Adjusted R-squared = 0.9472, and model p-value = 3.564e-10. The full output table from *R* is given in the Appendix.

Similarly to what is shown in Fig. 9 for the correction model for 3 pixels, we also derived the residual standard error for the r=5 pixel aperture correction model (Figure 12). Note that the model accuracy is slightly worse for r=5 pixels than for r=3 (residual error σ = 0.0326 and 0.0352, respectively). This is mainly due to the fact that the dataset for 5 pixel aperture is smaller. However, we stress that the difference in accuracy between the two models is not very large. When comparing the size of the error between the two models, the reader should keep in mind that the brightness reported on the x axis of Figs. 9 and 12 corresponds to electrons measured within two different aperture radii (3 and 5 pixels for Fig 9 and 12, respectively). Therefore, since we did not perform any aperture corrections, stars of a specific total brightness have about 15% more electrons (i.e. are shifted to the right) in Fig 12, as compared to Fig 9.

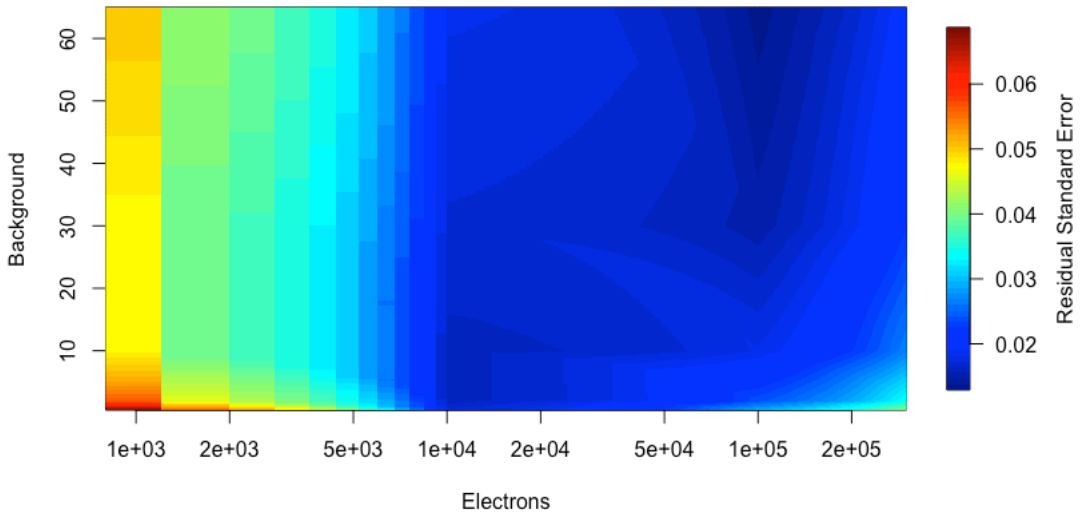

Figure 12 Residual standard error (in mag) of the model for r=5 pixel aperture radius, for MJD=59414. The x axis reports the stellar brightness in electrons (N e^- within r=5 pixel aperture). Y axis is background, in e^- per pixel.

5. Conclusions

We described the analysis of the External CTE monitor calibration program for data taken up to Cycle 28. A new model to correct CTE losses for point sources was derived. The new model takes into account of some recent findings, mainly concerning the curved dependence of CTE losses on stellar brightness on the image. The improved model allows for a more accurate correction within a large range of the parameter space covered by the observations, and provides both a more realistic and reasonable extrapolation to a wider range (i.e., very low background, very high brightness) not directly covered by the data.

For the most accurate results, we recommend aperture photometry with either a 5 or, better, a 3-pixel aperture radius, and correct the derived magnitude or flux using this improved model. A step-by-step guide on how to correct the data can be found in C12.

The CTE correction calculator is accessible at the ACS website, and can be found at the following URL: https://acsphotometriccte.stsci.edu/

6. Acknowledgments

MC thanks Jay Anderson for insightful discussions that helped to derive the new model. The authors thank Roberto Avila, Ralph Bohlin, Norman Grogin, Nimish Hathi and David Stark for providing useful comments. We thank Gagandeep Anand for substantial help with updating and improving the CTE web calculator.

7. References

Anderson, J. & Ryon, J., ACS-ISR 2018-04, *Improving the Pixel-Based CTE-correction Model for ACS/WFC*

Chiaberge, M, ACS-ISR 2012-05, *A New Accurate CTE Photometric Correction Formula for ACS/WFC*

Miles, N. & Chiaberge, M., ACS-TIR 2019-01, *photCTE: The Photometric CTE Pipeline for the ACS/WFC*

Pickel, J.C., Kalma, A.H., Hopkinson, G.R., and Marshall, C.J. 2003, IEEE Trans. Nucl. Sci. vol 50, 671.

R Core Team (2021). R: A language and environment for statistical computing. R Foundation for Statistical Computing, Vienna, Austria. URL https://www.R-project.org/.

Ryon, J, ACS-ISR 2018-09, *ACS/WFC Parallel CTE from EPER Tests*

Srour, J.R., Marshall, C.J., and Marshall, P.W. 2003, IEEE Trans. Nucl. Sci. vol 50, 653.

8. Appendix

In the following we report the full output tables from *R lm_robust* for both the 3- and 5-pixel aperture radii models (Tab. A1 and A2, respectively). More information is available at the reference webpage for the *R* function.

```
Coefficients:
                         Estimate Std. Error t value  Pr(>|t|)   CI Lower   CI Upper    DF
(Intercept)           -1.265e+00  1.533e-01  -8.254 1.528e-03 -1.702e+00 -8.287e-01 3.760
lsky                   9.257e-01  6.545e-02  14.142 1.128e-06  7.729e-01  1.078e+00 7.494
lf                     7.320e-02  2.226e-02   3.288 5.239e-02 -1.494e-03  1.479e-01 2.746
I(1/lf^2)             -4.179e+01  1.523e+00 -27.433 9.453e-09 -4.534e+01 -3.823e+01 7.444
lsky:lf               -6.833e-02  9.491e-03  -7.200 3.669e-04 -9.156e-02 -4.509e-02 5.987
lsky:I(1/lf^2)         2.127e+00  1.241e-01  17.135 2.724e-05  1.797e+00  2.456e+00 4.528
lf:I(1/lf^2)           5.375e+00  3.557e-01  15.111 8.955e-05  4.400e+00  6.350e+00 4.136
MJD:I(1/lf^2)          6.824e-04  2.424e-05  28.147 2.205e-08  6.249e-04  7.398e-04 6.906
lsky:lf:MJD:I(1/lf^2) -5.898e-05  2.793e-06 -21.117 4.970e-08 -6.547e-05 -5.248e-05 7.608

Multiple R-squared:  0.9624 ,   Adjusted R-squared:  0.9621
F-statistic:  2153 on 8 and 10 DF,  p-value: 3.677e-15
```

Table A1: Parameters and statistical significance of the curvilinear model for 3-pixel aperture radius photometry updated after the Cycle 28 Observations, from the *R* function *lm_robust*. Notations are as follows: lsky = Log(SKY), where SKY is the background level, lf = Log(F, brightness, in electrons), where electrons are measured within a 3-pixel aperture radius, MJD = modified Julian date of the observations. In the notation used in eq. (2), the intercept corresponds to a_9. Standard errors, t-statistics, lower/upper boundary of the confidence intervals and estimated degree of freedom for each coefficient are given. squared, F statistics and p-value for the fit are also reported. See the reference webpage for *lm_robust* in *R* for more details https://www.rdocumentation.org/packages/estimatr/versions/0.30.6/topics/lm_robust

```
Coefficients:
                         Estimate Std. Error t value  Pr(>|t|)   CI Lower   CI Upper    DF
(Intercept)           -1.684e+00  3.779e-01  -4.456 0.0073965 -2.669e+00 -6.992e-01 4.785
lsky                   9.454e-01  2.140e-01   4.419 0.0050678  4.151e-01  1.476e+00 5.697
lf                     1.192e-01  3.963e-02   3.008 0.0486021  1.277e-03  2.371e-01 3.413
I(1/lf^2)             -4.957e+01  5.697e+00  -8.702 0.0005687 -6.475e+01 -3.440e+01 4.479
lsky:lf               -7.861e-02  2.076e-02  -3.787 0.0096133 -1.298e-01 -2.745e-02 5.830
lsky:I(1/lf^2)         1.908e+00  4.762e-01   4.007 0.0080956  7.230e-01  3.093e+00 5.615
lf:I(1/lf^2)           6.616e+00  1.077e+00   6.143 0.0011150  3.932e+00  9.300e+00 5.583
MJD:I(1/lf^2)          7.895e-04  9.065e-05   8.709 0.0007896  5.418e-04  1.037e-03 4.173
lsky:lf:MJD:I(1/lf^2) -5.628e-05  1.090e-05  -5.161 0.0026322 -8.349e-05 -2.907e-05 5.556

Multiple R-squared:  0.9477 ,   Adjusted R-squared:  0.9472
F-statistic: 558.2 on 8 and 8 DF,  p-value: 3.564e-10
```

Table A2: Same as for Table A1, but for the 5-pixel aperture radius model.